NRIAG JOURNAL OF ASTRONOMY AND GEOPHYSICS
2021, VOL. 10, NO. 1, 290–299
https://doi.org/10.1080/20909977.2021.1918924

Taylor & Francis
Taylor & Francis Group

ARTICLE

OPEN ACCESS Check for updates

Assessment of spectra of solar radiation during the partial solar eclipse of 21 June 2020 at, Tanta, Egypt

U. Ali Rahoma, Samy A. Khalil, A.H. Hassan and A. A. Elminawy

Solar and Space Department, National Research Institute of Astronomy & Geophysics, Helwan, Cairo, Egypt

ABSTRACT

The main objective of this study is to obtain vartiation of solar spectrum during the recent solar eclipse in the range 350-1100nm. The net results are studying the spectral composition of global solar radiation which are collective of the direct and diffuse solar radiation values do not similar to the computation result (45% covering of the solar disk). The maximum absorption energy in the atmosphere is at range 820–900nm. The depression in the solar enerrgy is 0.11 ($W.m^{-2}.nm^{-1}$). The ultraviolet band is suffering low depression with respect to another bands but not given any risks on the human life as common. That the change in meteorological parameter related to variability in the solar spectrum that shift the short wave before 600 nmto long wave around 1000 nm. The most extreme drop in the solar spectrum lies in the interval which consists of the normal peak of the solar spectrum from 500 - 600nm. The percentage of radiant energy reaching the earth through 350-1100nm at the maximum of the solar eclipse was 54%. Consequently, the rate of depresion in energy is equal to 46%, which is very strange compared to the normal flow rate of 44%. During the eclipse, the maximum solar energy at the maximum eclipse are at 480nm (13.07 $W.m^{-2}.nm^{-1}$) and 630nm (13.17 $W.m^{-2}.nm^{-1}$). At the wavelength 580nm rpresents the absorbtion of O_2 , andthe absorbtion of H_2O at 680, 730, 780 and the maximum absorbtion energy by the H_2O is at 830nm (low enegy transimmted at 0.31 $W.m^{-2}.nm^{-1}$).

ARTICLE HISTORY
Received 22 February 2021
Revised 7 April 2021
Accepted 13 April 2021

KEYWORDS
Solar spectrum; partial solar eclipse; absorption bands

1. Introduction

Earth observation satellite spectrometer instruments designed to measure the particles and gases in the Earth's atmosphere. They depend upon the reflectance of the incident sunlight on the top-of-atmosphere (TOA) at various wavelengths in the UV, visible, near-infrared and shortwave-infrared spectral domains (Victor Trees et al. 2020). These TOA reflectances are calculated through the division of the measured Earth radiance by the measured solar irradiance. During a solar eclipse, the sun-oriented irradiance arriving at TOA is diminished as the Moon blocks (part of) the daylight, decreasing the Earth brilliance. Because the solar irradiance is commonly measured before the start of the eclipse, atmospheric measurements are distorted in the shadow of the Moon or, after raising an eclipse flag, undefined (Turner et al. 2018; Wang et al. 2008).

When the part of the sun is seen from Earth, a partial solar eclipse occurs in the Penumbra region of the earth, the degree of partiality depends on the distance of the observer from the edge of the umbra. Those who are closer to the path of totality will have near total darkness while those at the outer extremes of the penumbra will experience what approaches the clearness of the dawn or the twilight and the Sun's shape is like a new moon (Hassan and Rahoma 2002; Rahoma et al. 2004). When the moon is in its new phase, a total solar eclipse is occurring. The phenomenon starts when the moon is between the sun and the earth. Astronomical calculations can determine the time and place of past and future eclipses; this information is useful for dating historical events known to have occurred concurrently with an eclipse (Hassan et al. 2004; Yuldash and Yasser 2016; Masson et al. 2014; Kreifels et al. 2015).

Looking directly in the sun with naked eye raises the temperature of the retina by 4□ and may damage sensitive retinal cells. The use of using binoculars or telescopes can raise the temperature as much as 25□, resulting in serious thermal burns (Espenak 2014; Weniger et al. 2015). The component of the eclipse must produce a corresponding deformation of its shadow-cylinder cast in the direction of the line of light (Kchler et al. 2015; Die Sonnenfinsternis 2015: Vorschau auf das Strom system 2030 2015). Most solar and terrestrial radiation falls between 150 and 12,000 nm. The wavelengths in the visible region lie between 380 and 780 nm. The wavelengths of various electromagnetic waves cover a wide range. The change of the solar radiation spectral composition mainly depends on three factors: molecular scattering, which

CONTACT Samy A. Khalil samynki@yahoo.com National Research Institute of Astronomy & Geophysics, Solar and Space Department, Marsed Street, Helwan 11421, Cairo, Egypt.

is most intensive in the region of the short wave, aerosols scatter on large particles (dust, water droplets, etc.) and selective absorption by water vapour in the near infrared. In the ultraviolet range, ozone decisively affects the spectral composition of solar radiation (Buban et al. 2019; Burt 2018). The number of scientists has postulated that UV and blue light may contribute to retinal ageing and macular degeneration and UV and deep blue light have been shown to be damaging to the retina in laboratory studies. Epidemiological studies to date have not demonstrated any clear relationship, except possibly for some severe forms of the disease that seem associated with a history of greater blue light exposure (Kastendeuch et al. 2016; Lee et al. 2018; Liu et al. 2020; Mahmood et al. 2020).

(Ghitas and Sabry 2006) studied the variation of solar radiation with the current of mono-Si and a-Si solar cells sensors during the partial eclipse have been studied. Accordingly, the phase change of voltage-current of mono-Si cell during the short period of that eclipse has been plotted. Also, (Ghitas and Sabry 2006 and Espenak F.; Jay A. 2008) studied spectral behaviour of silicon solar cells under total solar eclipse of 29 March 2006. During the total solar eclipse, the effect of variation of both intensity and spectrum of solar radiation on the output response of the monocrystalline and amorphous silicon solar cells was investigated. The measurements of the eclipse data have yielded significant variation of spectral behaviour of monocrystalline and amorphous silicon solar cells, which explains spectral prediction of many observations of solar eclipse (Espenak F., Jay A. 2008; Maturilli and Ritter 2016).

During the last two decades, several authors performed extensive 3-D radiative transfer modelling of total solar eclipses, taking into account solar limb darkening (Nezval and Pavelka 2017; Ojobo et al. 2017; Pakkattil et al. 2020; Peñaloza-Murillo et al. 2020; Romano et al. 2017). The spectral behaviour of sunlight reaching a ground sensor located in or close to the total Moon shadow and the importance of the various (3-D) transfer radioactive components occurs in this work (Romano et al. 2017; Zerefos et al. 2000). The aim of this study is to obtain solar spectrum during the recent solar eclipse in the range 350–1100 nm.

Global Event: Annular solar eclipse at 21 June 2020, Local type: Partial solar eclipse, at Tanta duration is 01 h: 59 m (see Table 1), where at the maximum eclipse the air mass is 2.067 (m = sec θ), θ is the zenith angle.

The direct light of the solar radiation spectrum at both the top of the earth's atmosphere and at sea level, when the sun's surface temperature is approximately 5525 °K, the sun produces light with a similar distribution. Radiation interacts with matter in several ways: absorption, transmission, scattering, and reflection. Figure (1): clear that, the global solar spectral irradiance at the top of the atmosphere (top curve) and at the sea level (bottom curve), and note the attenuation resulting from absorption bands of gases and water vapour at sea level.

Table 1. Phases of the annular partial solar eclipse at Tanta, Egypt 21 June 2020.

Eclipse phases	First contact	Maximum	Last contact
L.M.T, hh: mm	06 h:25 m	07 h:21 m	08 h:22 m
Altitude of the sun, a	17.31°	28.92°	41.86°
Eclipse magnitude		00.43	

2. Data collection and methodology

The present study analyzes the effects of the 21 June 2020 partial solar eclipse from a different variation of solar spectrum.

2.1. Description of the data sets

Tanta, city, Lower Egypt, in the Nile River delta. It lies between on midway between the Rosetta (west) and Damietta (east) branches of the Nile on the Cairo-Alexandria superhighway. Industries include petroleum refining, cotton ginning, cottonseed oil extracting, wool spinning, flour milling, and the production of tobacco products and pasta (macaroni). The older Suez-Mediterranean oil pipeline runs through the Tanta city: 30°:47.61́ N, 30°:59.4́ E and 9 m Elev.

2.2. CCD camera (spectrometer)

The stellar net GREEN-Wave spectrometers can measure in 350–1150 nm wavelength range with an optical resolution of 0.2 nm and detector type of CCD −2048 pixels with a high speed 16-bit digitiser allows for fast data acquisition and a signal-to-noise of 400:1. The exposure time measurements were taken everyone millisecond and the wavelength steps every 0.4 nm.

2.2.1. Software used for spectroscopy

Spectroscopy Pro-tools lets you choose from a variety of colour palettes, the choose about to open in multiple plot windows, drag and drop spectral files, adjust line widths, legend and key text sizes, adjust background grids, hide and remove spectra with a click of a button, and adjust axis units quickly and easily.

2.3. Metrorological parameter, Tanta, Egypt

Air temperature is expected to range between the following values: Day: 36°C Night: 22°C. It is noted that,

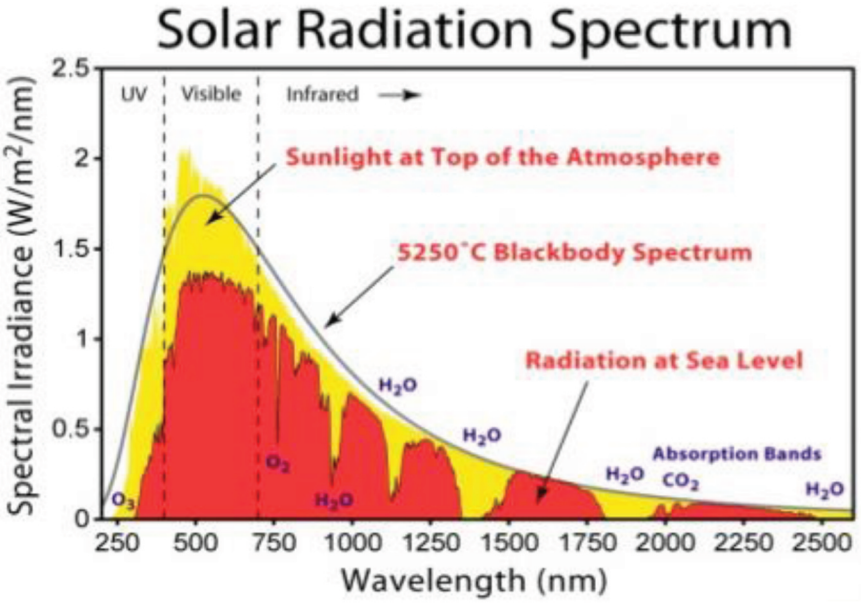

Figure 1. Simulated solar spectral irradiance at the top of the atmosphere and at sea level showing the attenuation due to gases and water vapour absorption bands in the atmosphere (Gueymard CA. 2019).

during the past, the following extreme values have been recorded: maximum record: 44°C, minimum record: 17°C. The maximum daily wind speed is expected to range between 7 Km/h and 21 Km/h.

Figure (2) and table (2): shows, the variation of air temperature and wind speed that: during the period of the partial solar eclipse from about 00:00–18:00 h o'clock am, we find a rise in air temperature with the stability of the wind speed, and the air temperature continues to rise after the eclipse has elapsed according to the weather changes occurring affected by the partial solar eclipse until the end of the day 21 June 2020.

As the air temperature rose during the period from 6 h: 00 m am to 12 h: 00 m am from 22 C° to 30 C° during the days of 20 and 22 June 2020 before and after the day of the partial solar eclipse.

Air quality scale, the ground-level of ozone can aggravate existing respiratory diseases and also lead to throat irritation, headaches, and chest pain O_3 is fair 39. Fine particulate matter are inhalable pollutant particles with a diameter less than 2.5 micrometres that can enter the lungs and bloodstream,

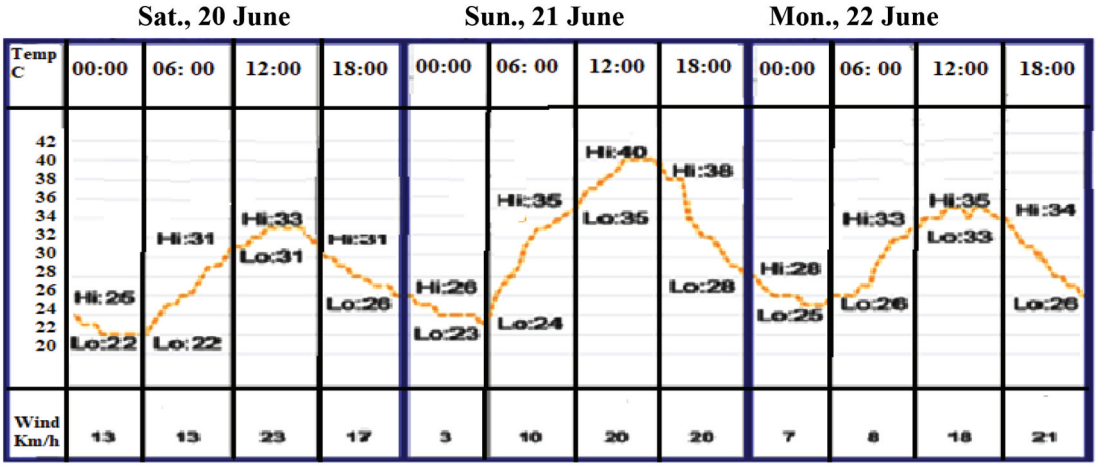

Figure 2. Air temperature (T) °C and wind speed (W) Km/h of observed data through the days 20, 21, and June 2020 (partial solar eclipse) Tanta, Egypt.

Table 2. The wind rose and direction of observed data through the days 20, 21, and June 2020 (partial solar eclipse) Tanta, Egypt.

N Northern	NE Northeast	E East	SE Southeast	S South	SW Southwest	W West	NW Northwest
34.9%	7.9%	0.3%	0%	1.7%	7.2%	13.7%	34.2%

resulting in serious health issues. The most severe impacts are on the lungs and heart. Exposure can result in coughing or difficulty breathing, aggravated asthma, and the development of chronic respiratory disease, is $PM_{2.5}$ is 82 μg/m^3 is fair, PM_{10}16 μg/m^3 is fair. Particulate Matter are inhalable pollutant particles with a diameter less than 10 micrometres. Particles that are larger than 2.5 micrometres can be deposited in airways, resulting in health issues (Masili and Ventura 2019).

3. Results and discussion

We have prepared a study that consists of studying the spectral changes in the different wavelengths using the spectrometer, which gives us results for changes in the range 25 nanometres, we found the following:

Figures (3–5): shows the intensity of the spectral solar radiation (W.m^{-2}.nm^{-1}) in the range 350–1100 nm for three sequin days 20 June (the day before the eclipse), 21 June (eclipse day) and 22 June 2020 (the day after the eclipse) for the same interval time of the partial solar eclipse (begin: 06 h:23 m am, maximum: 07 h:19 m am and the end: 08 h:33 m am) to compare the day of the eclipse with the one before it and after it.

Figure (6): shows the intensity variation of solar spectrum values (W.m^{-2}.nm^{-1}) of two days before and after partial solar eclipse (20 and 22 June) with the day eclipse during (21 June) at the maximum partial solar eclipse, 07 h:21 m am. To compare between the time of eclipse at 21 June and 2 days (20 and 22 June) for the same interval time, the depression values is about 0.1 W.m^{-2}.nm^{-1}, where the gap between them represents the energy lost due to the partial solar eclipse. The behaviour of the three curves is almost identical, which means that there is no significant change in the proportions of the atmospheric

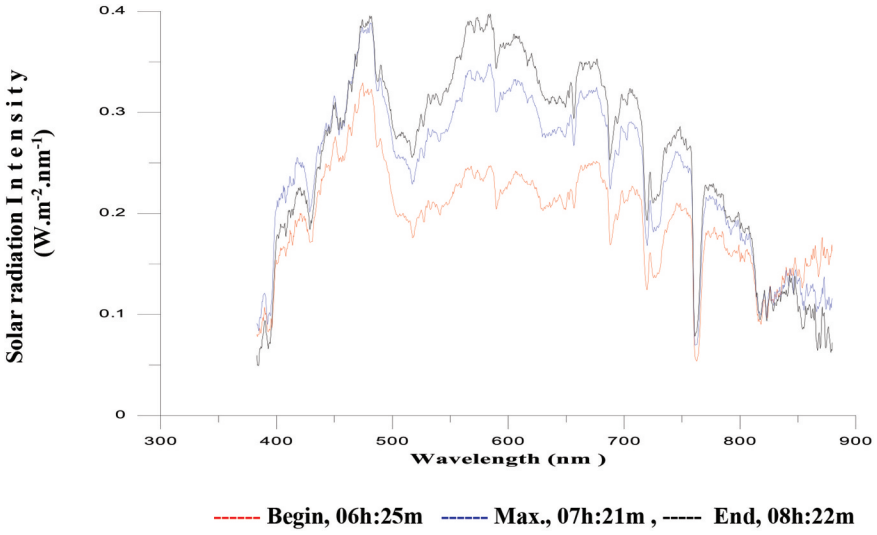

Figure 3. The intensity of the spectral solar radiation (W.m^{-2}.nm^{-1}) in the range 350–1100 nm at 20 June 2020 (before the day of partial solar eclipse).

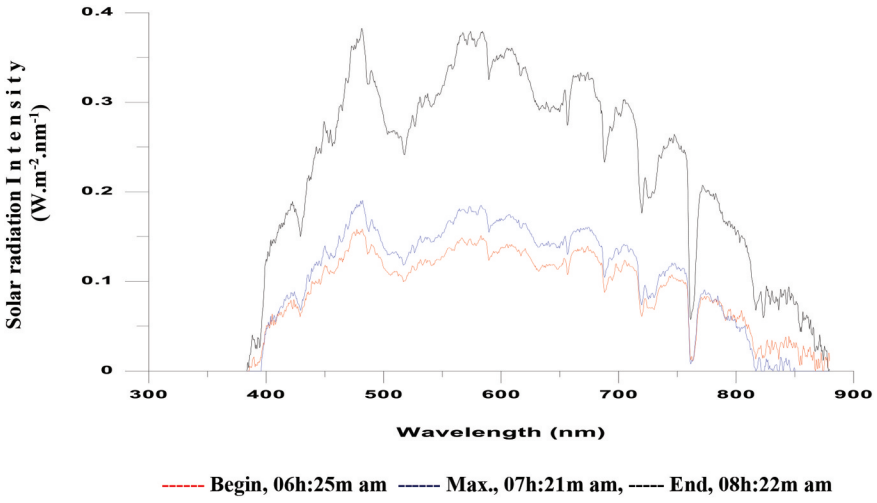

Figure 4. The intensity variation (W.m^{-2}.nm^{-1}) of the spectral solar radiation in the range 350–1100 nm during the at 21 June 2020 during the partial solar eclipse.

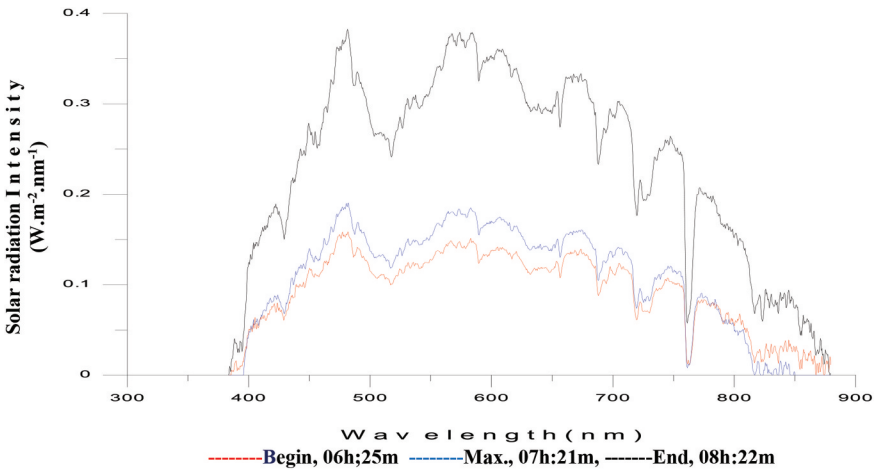

Figure 5. The solar radiation intensity variations ($W.m^{-2}.nm^{-1}$) of the spectral solar radiation in the range 350–1100 nm at 22 June 2020 (after the day of solar eclipse).

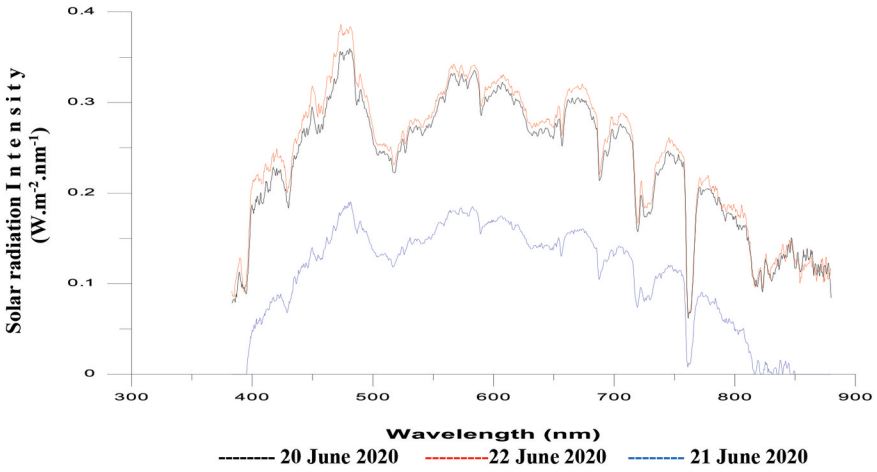

Figure 6. The intensity variation of solar spectrum values ($W.m^{-2}.nm^{-1}$) for three sequence days 20, 21, 22 June at the maximum partial solar eclipse at 07 h:21 m am.

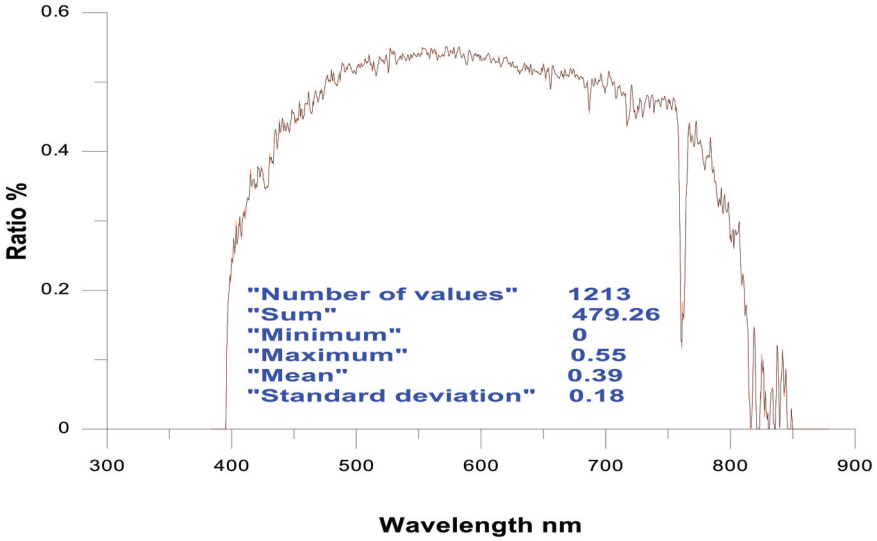

Figure 7. The intensity variation of solar spectrum ratio at maximum partial solar eclipse, 21 June 2020, at 07 h:21 m am, between the average values of two days (20 and 22 June) and the day of partial solar eclipse.

components, whether gaseous or dusty, for the same period of time for the 3 days. From all curves (figures. 3–6) clear that dealt with the dialect of the drought-based traffic in the 780 nm and the absorption of oxygen at 465–525 nm in the atmosphere, while in the other absorption regions it is H_2O are found in the spectrum and can be referred to figure (1) form to clarify this natural change in the atmosphere across oxygen absorption.

Figure (7): shows the intensity variation of solar spectrum ratio at maximum partial solar eclipse, 21 June 2020, at 07 h:21 m am (at air mass = 2.067), between the average values of two days (20 and 22 June) and the day of partial solar eclipse. It shows the decrease in the intensity of solar radiation during the solar eclipse on 21 June 2020, which reaches about 50% lower than the normal, this applies to the spectral range 400–800 nm and the maximum absorption energy in the atmosphere is at range 820–900 nm (for H_2O), except at the wavelength of 760 nm, which represents a higher percentage of water vapour at this time. Where the significant decrease is in the light range from 380 to 820 nm and the mean is 0.39 ± 0.18, this means that the absorption rates in the atmosphere are not equal depending on the components present.

Figure (8): shows the relationship between the mean of 2 days (20 and 22 June) of solar radiation intensity ($W.m^{-2}.nm^{-1}$) and the intensity of solar radiation for 21 June during the partial solar eclipse at the same interval time of the solar eclipse as: Y (mean of solar energy for two days 20, 22 June) = 0.11 + 1.247 (solar energy for 21 June), with correlation coefficient 0.9767. According the constant of equation in this relation, the depression in the solar energy during the eclipse is 0.11 ($W.m^{-2}.nm^{-1}$), which represents the difference between the day eclipse and the 2 days before and after for the same interval time, which corresponds to the result of the curve in a figure 6.

Figures (9–11): show the temporal change of 3D for the colour gradient intensity with the wavelength (nm)

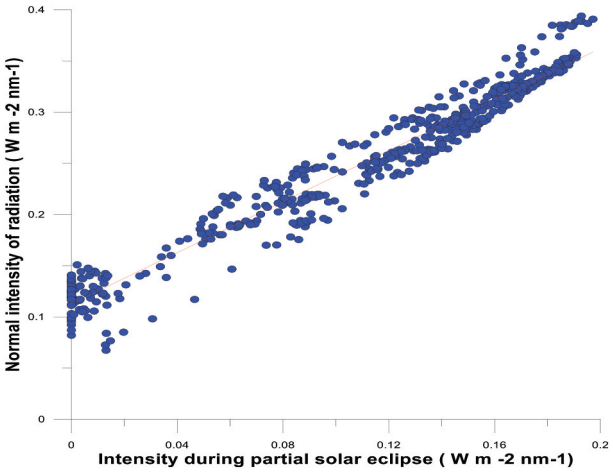

Figure 8. The relationship between the solar radiation intensity ($W.m^{-2}.nm^{-1}$) during the partial solar eclipse and mean of intensity of radiation for the day before and after (normal intensity of radiation) day of partial solar eclipse 21 June 2020.

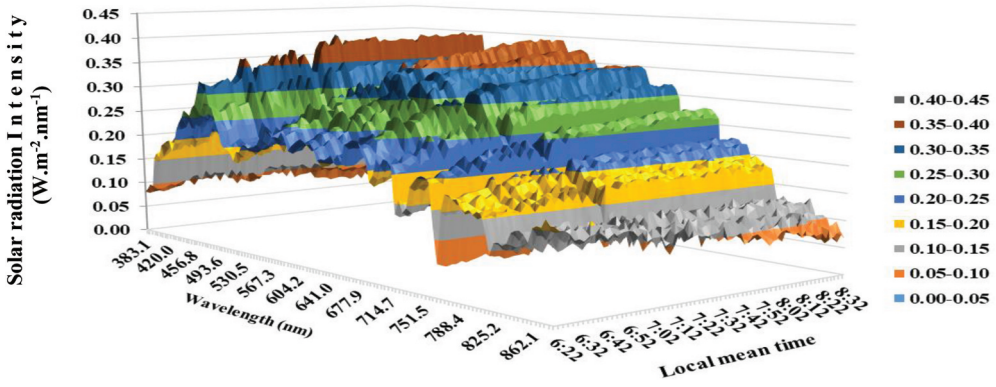

Figure 9. The variation of the spectral solar radiation intensity ($W.m^{-2}.nm^{-1}$) at 20 June 2020.

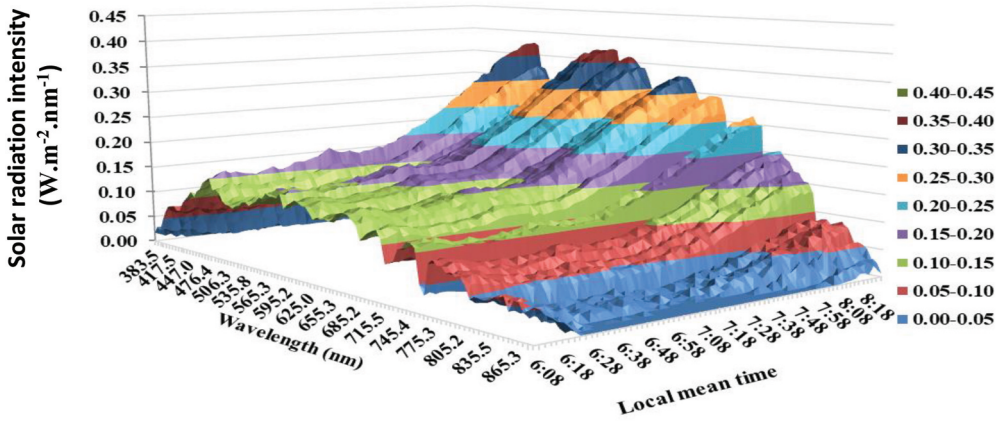

Figure 10. The variation of the spectral solar radiation intensity (W.m^{-2}.nm^{-1}) at the duration of partial solar eclipse 21 June 2020.

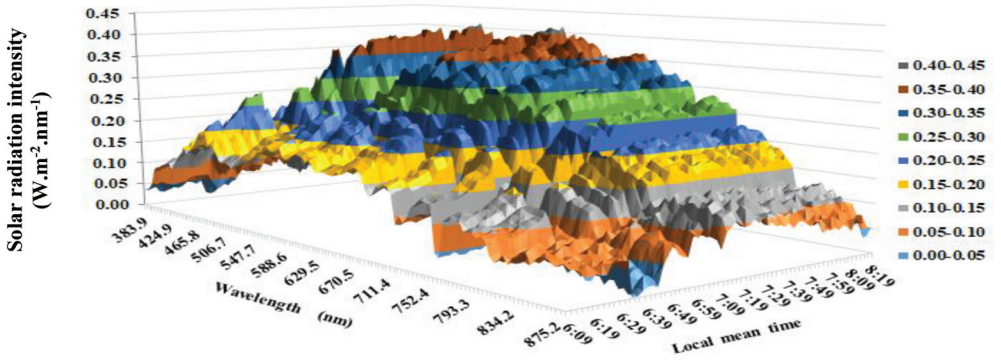

Figure 11. The change of the spectral solar radiation intensity (W.m^{-2}.nm^{-1}) on the following day of eclipse (22 June 2020).

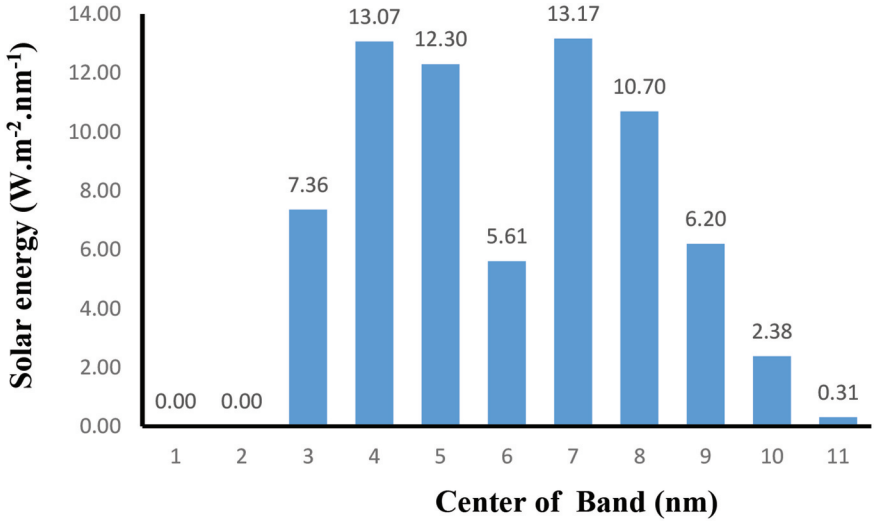

Figure 12. The variation of solar energy (W.m^{-2}.nm^{-1}) for nine solar spectrum bands during the partial solar eclipse 21 June 2020.

as the 0.05 W.m^{-2}.nm^{-1} steps at 20 June (the day before the eclipse), 21 June (eclipse day) and 22 June 2020 (the next day of the eclipse) during 06 h:25 m to 08 h:22 m.

It is clear that the great similarity in the colour gradient of the intensity and ratios for the days of 20 and 22 June, while the difference is clear for the same time period of 21 June, especially the reality between 400 and 700 nm for the energy depression range 0.15–0.25 W.m^{-2}.nm^{-1}. Figure (12): shown the distributions of the total energy in any band for 11 solar intensity radiation spectrum bands (W.m^{-2}.nm^{-1}) during the partial solar eclipse 21 June 2020. Based on these figures (9–11), the attenuation of solar radiation observations during the partial solar eclipse (45%) could not see here because the observations are taken

Table 3. The variation of solar energy ($W.m^{-2}.nm^{-1}$) at the certain band wavelength according figure 12 and [34].

	3	4	5	6	7	8	9	10	11
Centre of band (nm)	430	480	530	580	630	680	730	780	830
Solar energy	07.36	13.07	12.30	05.61	13.17	10.70	06.20	02.38	0.31
Absorbtion gases	O_3			O_2		H_2O	H_2O	H_2O	H_2O

of the spectral composition of the global solar radiation that collective of the direct and diffuse solar radiation values. The increase in the solar radiation intensity on the interval wavelength from 350 to 450 nm, which lies in the end of the ultraviolet solar radiation. The minimum values of the spectrum is lies between 450 and 550 nm, which represents the maximum absorption in the atmosphere spectrum and this region represents the normal of maximum peak of the solar spectrum, and go to up from 700 to 900 nm which is between related to the near infrared interval and down in the deep infrared from 900 nm to the end. Also; the solar spectrum which lies before the 500 nm go to increase in the intensity of solar radiation, but not more the normal this interval represented the end of ultraviolet solar radiation. That means some increasing in the ultraviolet solar radiation but it is high effective at the human life as it is diffusion in the news during the solar eclipse. The maximum drop in the solar spectrum lies in the interval that consists of the normal peak of the solar spectrum range 500–600 nm. With respect to the end of the ultraviolet solar radiation that lies before wavelength equal 400 nm we can say that; the ultraviolet bands is suffered high depression but not given any risks on the human life as common.

Table (3): represents the percentage values of solar energy at each light band during the duration of the eclipse. From figure (12) and table (3), the maximum energy are 13.07 and 13.7 ($W.m^{-2}.nm^{-1}$) around 480 nm (green) and 630 nm (red), this mean that, at two centre wavelength these are high air transmittance, and when compared with figure 1 and (NASA 1980) to find out the absorption regions and around air mass 2, the values of energy are: 7.36 ($W.m^{-2}.nm^{-1}$) at 430 nm represents the absorption of O_3, 5.61 ($W.m^{-2}.nm^{-1}$) at 580 nm represents the absorption of O_2, and the absorption of H_2O at 680, 730, 780 and the maximum absorption energy by the H_2O is at 830 nm (low enegy transmitted at 0.31 $W.m^{-2}.nm^{-1}$). Then, the results of the solar irradiance values for different wave spectra from 350 to 1150 nm at a rate of 25 nm for each period by the average of the result values for the same time period observed for the peak of the eclipse at time 07 h:21 m am, the peak rate reaches 54% (46% depression).

4. Conclusion

The net result is that studying the spectral composition of global solar radiation, which is a collective of the direct and diffuse solar radiation values do not similar to the computation result (45% covering of the solar disk). It shows the decrease in the intensity of solar radiation during the solar eclipse on 21 June 2020, which reaches about 50% lower than normal. This applies to the spectral range 400–800 nm. The maximum absorption energy in the atmosphere is at range 820–900 nm. The depression in the solar energy is 0.11 ($W.m^{-2}.nm^{-1}$), which represents the difference between the day eclipse and the mean of 2 days before and after for the same interval time.

Increase in the whole different local mean times in the interval 350–450 nm but without risks on the human eye; that interval lies in the end of the ultraviolet solar radiation. The minimum lies between 500 and 700 nm this interval are represented the normal maximum peak of the solar spectrum, and goes up from 700 to 900 nm, which related to the infrared interval and down in the deep infrared from 900 nm to the end. The ultraviolet band is suffering low depression with respect to another bands but not given any risks on the human life as common. That the change in meteorological parameter related to variability in the solar spectrum that shift the short wave before 600 nm to the long wave around 1000 nm. The maximum drop in the solar spectrum lies in the interval which consists of the normal peak of the solar spectrum from 500 to 600 nm. The percentage of radiant energy reaching the earth through 350–1100 nm at the maximum of the solar eclipse was 54%. Consequently, the rate of depression in energy is equal to 46%, which is very strange compared to the normal flow rate of 44%. During the eclipse, the maximum solar energy at the maximum eclipse are at 480 nm (13.07 $W.m^{-2}.nm^{-1}$) and 630 nm (13.17 $W.m^{-2}.nm^{-1}$). At the wavelength 580 nm rpresents the absorption of O_2, and the absorption of H_2O at 680, 730, 780 and the maximum absorption energy by the H_2O is at 830 nm (low enegy transmitted at 0.31 $W.m^{-2}.nm^{-1}$).

Disclosure statement

No potential conflict of interest was reported by the author(s).

References

Buban MS, Lee TR, Dumas EJ, Baker CB, Heuer M. 2019. Observations and numerical simulation of the effects of the 21 August 2017 North American total solar eclipse on surface conditions and atmospheric boundary-layer evolution. Bound-Layer Meteorol. 171(2):257–270. doi:10.1007/s10546-018-00421-4.

Burt S. 2018. Meteorological impacts of the total solar eclipse of 21 August 2017. Weather. 73(3):90–95. doi:10.1002/wea.3210.

Die Sonnenfinsternis 2015: Vorschau auf das Strom system 2030. Herausforderungen f_r die stromversorgung in systemen mit hohen anteilen a wind- und solar energie": c. Redl, B. Praetorius in Agora Energie wende, Berlin, 2015. accessed on 2015 Apr 10. http://www.agoenderaenergiewde/fileadmin/downloads/publikationen/Hintergrund/Sonnenfinsternis_2015/Agora_Sonnenfinsternis_web_16032015.pdf

Espenak F, "Total solar eclipse of 2015 march 20": national aeronautics and space administration (NASA). 2014, accessed 2015 Apr 14. http://eclipse.gsfc.nasa.Gov .\

Ghitas A, Sabry M. 2006. Spectral behaviour of silicon solar cells under total solar eclipse of 29 March 2006. NRIAG J Astron Astrophysics. 71–84.

Gueymard CA. 2019. The SMARTS spectral irradiance model after 25 years: new developments and validation of reference spectra. Solar Energy. 187:233–253. doi:10.1016/j.solener.2019.05.048.

Hassan AH, Rahoma UA, The depression of different solar radiation components During the solar eclipse 11 August, Egypt, World Conference on Technology Advances for Sustainable Development Gezirah Sheraton, Cairo - Egypt, 11-14 March 2002.

Hassan AH, Shaltout MA, Rahoma UA. 2004. The depression of different solar radiation components during the solar eclipse 11 August 1999 over Egypt. J Astronomical Society Egypt. 12/I:70–81.

Jay A. EF, Total Solar Eclipse of 2008 August 01 - Parameters, NASA, (July 2004), Retrieved 2008 Aug. 9.

Kastendeuch PP, Najjar G, Colin J, Luhahe R, Bruckmann F. 2016. Effects of the 20 March 2015 solar eclipse in Strasbourg, France. Weather. 71(3):55–62. doi:10.1002/wea.2673.

Kchler C, Steiner A, Lee D, Thieler J, Saint-Drenan Y-M, Ernst D, Zirkelbach M, Ritter B, submitted, 2015.

Kreifels N, Killinger S, Mayer J, Moller B, Wittwer C, Burger B, Roth W, Biener W. 2015. Sonnenfinsternis am 20. M. 2015. Auswirkungen auf die Systemstabilit_t der deutschen Stromversorgung.,Freiburgi.Br. accessed on 2015 Mar 18. https://www.ise.fraunhofer.de/de/veroeffentlichungen/veroefentlichungen-pdf-dateien/studien-und-konzeptpapiere/studie_sonnenfinsternis.pdf

Lee TR, Buban M, Palecki MA, Leeper RD, Diamond HJ, Dumas E, Meyers TP, Baker CB. 2018. Great American Eclipse data may fine-tune weather forecasts. Eos. 99:2018. doi:10.1029/2018EO103931.

Liu Y, Elmhamdii A, Al-Trabulsy H, Song T, Zhang X. 2020. A magnificent ring of fire on the horizon of the Persian Gulf: the annular eclipse of Saudi Arabia on December 26, 2019. Amateur Astronomers. 7:57–60.

Mahmood R, Schargorodski M, Rappin E, Griffin M, Collins P, Knupp K, Quilligan A, Wade R, Cary K, Foster S. 2020. The total solar eclipse of 2017: meteorological observations from a Statewide Mesonet and Atmospheric Profiling Systems. Bull Am Meteorol Soc. 101(6):E720–E737. doi:10.1175/BAMS-D-19-0051.1.

Masili M, Ventura L. 2019. Local tilt optimization of photovoltaic solar panels for maximum radiation absorption. Int J Photoener. 2019:1–10. Hindawi Limited. doi:10.1155/2019/3254780.

Masson G, Orlandi S, Rekinger M. 2014. Global market outlook for photovoltaics 2014 –2018, report by the european photovoltaic industry association (EPIA). 2014-2018, Medium Res. pdf) 2015. http://www.cleanenergybusinesscouncil.com/site/resources/files/reports/EPIA_Global_Market_Outlook_for_Photovoltaics

Maturilli M, Ritter C. 2016. Surface radiation during the total solar eclipse over Ny-Ålesund, Svalbard, on 20 March 2015. Earth System Sci Data. 8(1):159–164. doi:10.5194/essd-8-159-2016.

NASA. spectral distribution of solar radiation, technical memorandum 82021. (1980).

Nezval O, Pavelka M. 2017. Microclimate changes in a spruce stand and meadow ecosystem during a solar eclipse in the Czech Republic. Weather. 72(3):67–72. doi:10.1002/wea.2802.

Ojobo E, Okoh D, Okeya D, Yusuf N, Adukwu G. 2017. The response of meteorological parameters to the September 1 2016 solar eclipse as observed in Anyigba, Nigeria. J Space Sci Technol. 6(1):16–24.

Pakkattil A, Muhsin M, John S, Saseendran A, Thomas AP, Deepa V, Varma R. 2020. Trace pollutant fluctuations observed in Calicut city, India, during the annular solar eclipse on 26 December 2019. Atmos Pollut Res. 11 (11):2049–2055. doi:10.1016/j.apr.2020.07.026.

Peñaloza-Murillo MA, Roman MT, Pasachoff JM. 2020. Anomalies and fluctuations of near surface air temperature at Tianhuangping (Zhejiang), China, produced by the longest total solar eclipse of the 21st century under cloudy skies. Publ Astron Soc Pac. 132(1017):20. doi:10.1088/1538-3873/abb2f9.

Rahoma UA, Shaltout MA, Hassan AH. 2004. Study of spectral global solar radiation during the partial solar eclipse of 11 August 1999 at Helwan, Egypt. J Astronomical Society Egypt. 12/I:31–45.

Romano S, Lo Feudo T, Calidonna CR, Burlizzi P, Perrone MR. 2017. Solar eclipse of 20 March 2015 and impacts on irradiance, meteorological parameters, and aerosol properties over southern Italy. Atmos Res. 198:11–21. doi:10.1016/j.atmosres.2017.08.001.

Trees V, Wang P, Stammes P. 2020. Restoring the top-of-atmosphere reflectance during solar eclipses: a proof of concept with the UV Absorbing Aerosol Index measured by TROPOMI. Atmo Chem Phys. doi:10.5194/acp-2020-1172

Turner DD, Wulfmeyer V, Behrendt A, Bonin TA, Choukulkar A, Newsom RK, Brewer WA, Cook DR. 2018. Response of the land-atmosphere system over north- central Oklahoma during the 2017 eclipse. Geophy Res Letter. 45 (3):1668–1675. doi:10.1002/2017GL076908.

Wang P, Stammes P, Van Der A, R., Pinardi G, Van Roozendael M. 2008. FRESCO+: an improved O_2 A-band cloud retrieval algorithm for tropospheric trace gas retrievals. Atmo Chem Phys. 8(21):6565–6576. doi:10.5194/acp-8-6565-2008.

Weniger J, Bergner J, Tjaden T, Quaschning V. Einfluss der Sonnenfinsternis im M_rz 2015 auf die Solar stromerzeugung in Deutschland, Berlin, 2014. accessed 2015 Jan 20. https://pvspeicher.htw-berlin.de/wp-content/uploads/2014/10/HTW-Berlin-Studie-Einfluss-der-onnenfinsternisim-M%C3%A4rz-2015-auf-die-Solarstromer-zeugung-in-Deutschland.Pdf

Yuldash S, Yasser A. 2016. Abdel-hadi, influence of the solar eclipse on the power and operational Parameters of the big solar furnace in parkent of Uzbekistan, International. J Energy Smart Grid. 1(1).

Zerefos CS, Balis DS, Meleti C, Bais AF, Tourpali K, Kourtidis K, Vanicek K, Cappellani F, Kaminski U, Colombo T, et al. 2000. Changes in surface solar UV irradiances and total ozone during the solar eclipse of August 11, 1999. J Geophys Res Atmos. 105(26):463–26 473. doi:10.1029/2000JD900412.